



HAL
open science

Combining Polyester-Based Solid Polymer Electrolytes with Lithiated Organic Cathodes for 3.5 V-Class Li-Organic Rechargeable Batteries

Aswadh Shyma Sajeevan, Lou Bernard, Pierre Tran-Van, Daniel Brandell,
Stéven Renault, Philippe Poizot

► **To cite this version:**

Aswadh Shyma Sajeevan, Lou Bernard, Pierre Tran-Van, Daniel Brandell, Stéven Renault, et al.. Combining Polyester-Based Solid Polymer Electrolytes with Lithiated Organic Cathodes for 3.5 V-Class Li-Organic Rechargeable Batteries. ACS Applied Polymer Materials, 2024, 10.1021/ac-sapm.4c00511 . hal-04604419

HAL Id: hal-04604419

<https://hal.science/hal-04604419v1>

Submitted on 7 Jun 2024

HAL is a multi-disciplinary open access archive for the deposit and dissemination of scientific research documents, whether they are published or not. The documents may come from teaching and research institutions in France or abroad, or from public or private research centers.

L'archive ouverte pluridisciplinaire **HAL**, est destinée au dépôt et à la diffusion de documents scientifiques de niveau recherche, publiés ou non, émanant des établissements d'enseignement et de recherche français ou étrangers, des laboratoires publics ou privés.

Combining Polyester-based Solid Polymer Electrolytes with Lithiated Organic Cathodes for 3.5 V-Class Li-Organic Rechargeable Batteries

Aswadh Shyma Sajeevan,^{a,b} Lou Bernard,^{a,c} Pierre Tran-Van,^c Daniel Brandell,^d

Stéven Renault,^a Philippe Poizot^{a,}*

^a Nantes Université, CNRS, Institut des Matériaux de Nantes Jean Rouxel, IMN, F-44000 Nantes, France

^b ALISTORE-European Research Institute, 80000 Amiens, France

^c Technocentre Renault, 1 Avenue du Golf, 78280 Guyancourt, France

^d Department of Chemistry–Ångström Laboratory, Uppsala University, SE-751 21 Uppsala, Sweden

ABSTRACT

Solid-state batteries have attracted intensive attention in recent years for their potential to overcome the limitations of conventional liquid-electrolyte batteries while allowing for compatibility with lithium metal electrodes and improving energy density. On the other hand, there is a growing interest in developing organic electrode materials to supplement existing technologies while offering sustainable, versatile and potentially low-cost electrochemical storage devices. In this study, we report the first solid-state Li polymer batteries based on poly(ϵ -caprolactone-co-trimethylene carbonate) 80:20 random copolymer with 28 wt.% LiTFSI as the electrolyte paired with high-potential lithiated organic insertion materials namely both magnesium and zinc (2,5-

dilithium-oxy)-terephthalate compounds. This polymer electrolyte showed to be compatible with the organic electrode, and functional cells could be constructed. The zinc derivative was selected due to the high ionic potential value of Zn^{2+} , similar to that of Mg^{2+} , and was synthesized in methanol using a scalable and efficient two-step chemical process. The electrochemical study pointed out an optimal operation temperature of 60 °C for such solid-state Li polymer batteries compared to the use of conventional carbonate-based liquid electrolytes at 23 °C. A better stability upon cycling was observed with the magnesium-based phase while the zinc counterpart shown more pronounced capacity loss, requiring further investigations.

KEYWORDS: organic battery, solid polymer electrolyte, polyester electrolyte, lithiated organic cathode, carboxyphenolate, dihydroxyterephthalate salts

Introduction

The revolution in the field of battery technology began with the commercialization of lithium-ion batteries (LIBs) by Sony in 1991 by offering batteries with significantly higher energy density and longer lifespans than their predecessors.¹ The versatility of LIBs has now reached beyond the portable electronics industry to broader applications like electric vehicles (EVs) and smart grids.² However, the huge advancement in this field is not reflected in the development of sustainable and renewable technologies within the battery sector. As the global community is shifting towards a more sustainable and environment-friendly future, the field of battery technology will be confronted with a necessity for substantial transformation, as underlined by one of us more than 10 years ago.³ The current commercial LIBs are predominantly based on finite natural resources like cobalt and nickel.⁴ The mining and extraction process of these materials not only contributes to ecological degradation but also raises concerns about the long-term viability of these resources. This justifies the potential use of organic electrode materials (OEMs) as a relevant alternative capable of solving the problem at its root.^{5,6} Unlike conventional transition metal oxide-based electrode materials, OEMs can be derived from biomass resources or other inexpensive organic compounds through relatively benign processes, which makes them relatively inexpensive.⁷⁻¹³ Owing to the enormous design flexibility,¹⁴ OEMs can be synthesized and modified with a wide range of structures and functionalities, making the operation in different electrolyte media possible. Numerous reviews on the topic are now available in the literature, see for example Refs.^{5,15-24}.

The conventional liquid electrolytes hinder the implementation of greener technologies like OEMs due to their high solubility, often leading to a rapid decay in capacity. The liquid electrolytes also hinders the employment of lithium metal negative electrodes, which offer lower

operating potential and almost tenfold higher capacity than conventional electrodes like graphite.^{16,25} In general, lithium metal electrodes exhibit pronounced reactivity in traditional liquid electrolytes, leading to non-uniform lithium deposition and subsequent formation of lithium dendrites; this process not only depletes the electrolytes but also significantly contributes to capacity fading and causes short circuits.^{25,26} Solid-state electrolytes, both ceramic and polymeric, are potential alternatives that can mitigate these concerns raised by liquid electrolytes. Even though ceramic solid-state electrolytes are chemically and mechanically robust, they often contain expensive and less-abundant elements like lanthanum, germanium, etc., and are synthesized through very high-temperature processing techniques. On the other hand, akin to OEMs, solid polymer electrolytes (SPEs) are composed of inexpensive and naturally abundant elements.⁵ In addition, they offer a high degree of mechanical flexibility that facilitates the fabrication of batteries in any required geometry. Although many polymer materials cannot be classified entirely as nonflammable, they exhibit less chance of thermal hazards due to their negligible vapor pressure. Due to these reasons, SPEs opens up a potential avenue towards a comparatively safer and better energy storage solutions. This technology deserves much more attention and rigorous studies to unlock its full potential.

In 1978, Michel Armand introduced the concept of implementing solid polymer electrolytes in batteries.²⁷ Indeed, such pioneering efforts mainly on poly(ethylene oxide) (PEO) based electrolytes paved the direction for the realm of SPE research.²⁸⁻³¹ Polyether-based electrolytes especially PEO have been a benchmark SPE research for decades, due to their low glass transition temperature and reasonable ionic conductivity at the higher temperature range with the addition of different lithium salts.^{32,33} A number of studies have been conducted to improve this SPE through crosslinking,³⁴ the addition of plasticizers,³⁵ varying lithium salt concentration,³⁶

and other chemical strategies.³⁷ Interestingly, this solid-state battery configuration not only alleviates some of the challenges associated with liquid electrolytes but also paves the way for promising advancements in molecular and eco-friendly energy solutions.³⁸ Since the early 2000s, the Bolloré group, alongside *BlueSolutions*, has fueled the research in Lithium Metal Polymer (LMP[®]) batteries, based SPEs. This relatively mature technology has been deployed to power EVs since 2011 and is now globally commercialized across various mobility and stationary storage domains. The first attempts to integrate OEMs directly into the LMP[®] technology demonstrated the feasibility of organic insertion materials to be cycled, however, several constraints brought about by the high operating temperature (80 to 100 °C), above the melting point of the SPE.^{39,40} Hence, it makes sense to investigate fully amorphous polymers, like poly(ϵ -caprolactone-co-trimethylene carbonate) (PCL-PTMC), which offers a promising alternative to PEO-based counterparts. At lower temperatures, this copolymer outperforms PEO in terms of lithium or sodium conductivity, while displaying very high cationic transference numbers and promising battery cycling capability. Poly(ϵ -caprolactone) (PCL) has a low glass transition temperature near -65°C , but is semi-crystalline. In contrast, poly(trimethylene carbonate) (PTMC) is completely amorphous, with a glass transition temperature of around -15°C , thereby offering lower ionic conductivity. Copolymerization can merge the attributes of these distinct polymers and render a polymer with the desired characteristics of amorphicity and low T_g . A significant improvement is achieved when introducing 20 mol% PTMC to PCL, creating a random copolymer. This modification significantly reduces the crystallinity of the host material, and the addition of salt effectively removes any residual crystallinity. Through the application of this copolymer, Mindemark and co-workers have demonstrated enhanced cycling stability at ambient temperature using low-voltage positive electrode materials such as LiFePO_4 .^{41,42}

Within this context, we decided to take benefit of our recent developments in synthesizing high-potential lithiated OEMs to fabricate and electrochemically assess a new design for a Li-organic rechargeable battery using a solid polyester-polycarbonate electrolyte able to operate at comparatively lower temperature (≤ 60 °C) compared to the LMP[®] technology (80-100 °C range). In practice, we have implemented magnesium (2,5-dilithium-oxy)-terephthalate (Mg(Li₂)-*p*-DHT) as positive insertion material⁴³ as well as the corresponding zinc counterpart phase (Zn(Li₂)-*p*-DHT) in a Li-metal SPE-based cells for the first time. The OEMs have been selected due to their high operating potential ($\langle E \rangle \approx 3.45$ V vs Li⁺/Li) similar to that of LiFePO₄.

Experimental Section

General Methods

Fourier-transform infrared spectroscopy (FTIR) measurements using KBr pellets were recorded on a FTIR Bruker Vertex 70 in the range 4000 - 400 cm⁻¹ with a resolution of 4 cm⁻¹. Air-free pellets were prepared in an argon glove box by mixing the sample at 1 wt.% with spectroscopic-grade potassium bromide. Direct measurements of polymer samples were recorded using Bruker ALPHA Platinum-ATR FTIR Spectrometer in the same range. ¹H liquid NMR spectra were recorded on a Bruker AVANCE III 400 MHz. Chemical shifts (δ) were calibrated using the residual peak of the reference deuterated solvent (2.50 ppm for DMSO-d₆). NMR solvents used were purchased from Eurisotop (purity higher than 99.9%). Both Zn and Li contents were precisely determined by Inductively Coupled Plasma-Atomic Emission Spectroscopy (ICP-AES) using an iCAP 6300 radial analyzer (Thermo Scientific). A mono-element solution of Zn and Li (1000 ppm, CHEMLAB) were used for the calibration. The X-ray powder diffraction patterns of

the materials were measured on a Bruker D8 Advance diffractometer in Bragg-Brentano geometry with Cu $K\alpha_1$ radiation. The thermogravimetry-differential scanning calorimetry (TG-DSC) experiments of powder samples were performed under argon with a SENSYS_{Sevo} instrument from Setaram using a heating rate of 5 °C min⁻¹ up to 800°C. The polymer was evaluated through thermogravimetric analysis (TA Instruments Q500), from room temperature up to 500 °C at a heating rate of 10 °C min⁻¹, under nitrogen atmosphere and DSC (using TA Instruments Q20) from -80 °C to 130 °C at a rate of 10 °C min⁻¹ under nitrogen atmosphere. Scanning Electron Microscopy (SEM) was performed on a JSM-7600F from JEOL.

Chemicals

2,5-dihydroxyterephthalic acid (H_4 -*p*-DHT, Sigma-Aldrich, 98.0 %), zinc(II) bis(trifluoromethane sulfonyl)imide) ($Zn(TFSI)_2$, Solvionic, 99.5 %), lithium bis(trifluoromethane sulfonyl)imide) ($LiTFSI$, Solvionic, 99.5 %), lithium methoxide solution ($MeOLi$, Sigma Aldrich, 2.2 M in methanol), trimethylene carbonate (TMC, Richman Chemicals, 99 %), stannous 2-ethylhexanoate (95 %, Sigma-Aldrich), anhydrous methanol ($MeOH$, Thermo Scientific 99.9 %), anhydrous acetonitrile (ACN, Sigma-Aldrich, 99.8%), anhydrous toluene (Acros Organics, 99.8%), were used as received without further purification and stored in an argon-filled glovebox. ϵ -Caprolactone (CL, Perstorp, 99 %) was distilled under reduced pressure over CaH_2 (Sigma-Aldrich, 99.9 %) and stored in an argon-filled glovebox. Ketjenblack EC-600JD (AkzoNobel) and C-ENERGY SUPER C65 (Imerys) were used as conducting carbon additive for the preparation of the composite positive electrodes.

*Synthesis of zinc (2,5-dilithium-oxy)-terephthalate ($Zn(Li_2)$ -*p*-DHT)*

The synthesis of Zn(Li₂)-*p*-DHT was entirely performed in an argon-filled glovebox. Into a homogeneous solution of H₄-*p*-DHT (1.0 g, 5.1 mmol, 1 eq.) in anhydrous MeOH, (200 mL) prepared in a round bottom flask, 9.3 mL of MeOLi (2.2 M in methanol, 20.4 mmol, 4 eq.) was dripped. A homogeneous light yellow colored solution was immediately obtained and kept for stirring at room temperature for 1 h. 3.17 g of Zn(TFSI)₂ (5.1 mmol, 1 eq) were then added to the solution. Finally, the flask was sealed, heated up to 60 °C and kept stirring for 16 h. A yellow precipitate was immediately formed and turned orange while heating. The solution was centrifuged at 6500 rpm for 30 min to separate the precipitate and washed with 4 × 100 mL methanol. The as-prepared solid was dried under vacuum at room temperature overnight. Finally, the sample was subjected to a thermal treatment at 130 °C for 16 h under vacuum in a drying glass oven (BüchiB-585 glass oven for drying) to obtain pure Zn(Li₂)-*p*-DHT as an orange powder (yield: 85 %). The absence of residual methanol was confirmed using thermal analysis and IR spectra. FTIR (cm⁻¹): 1600-1575 (ν_{as} OC-O⁻), 1468-1411 (ν C=C), 1364 (ν_s OC-O⁻), 1199 (ν C-OLi), 878-809 (ν C-H tetra-substituted benzene). ¹H NMR (400 MHz, DMSO-d₆ + few drops of H₂SO₄)⁸ δ (ppm) = 7.15 (2H, s), 7.14 (2H, s); ¹³C NMR (100 MHz, DMSO-d₆ + few drops of H₂SO₄): δ (ppm) = 171.3 (COOH), 153.0 (C-OH), 120.7 (C-COOH), 118.6 (CH). Elemental analysis (calculated, found) (wt. %): Zn (23.92 wt.%, 23.45 ± 0.07 wt.%, Li (5.08 wt%, 5.24% ± 0.22 wt.%). Further details are reported in SI.

Synthesis of poly(ε-caprolactone-co-trimethylene carbonate) copolymer and preparation of polymer electrolyte film

Synthesis of the copolymer poly(ε-caprolactone-co-trimethylene carbonate) (PCL-PTMC) and fabrication of the resulting SPE films, involving a solvent casting technique, have been reported elsewhere.⁴¹ The formulation included a 28 wt.% concentration of lithium

bis(trifluoromethane)sulfonamide (LiTFSI), calculated based on the total weight of the solid constituents, excluding the solvent. The entire process was conducted in an argon-filled glovebox. Post-casting, the films were stacked between Teflon[®] sheets, hot pressed at 60 °C to obtain the desired thickness ($\approx 200 \mu\text{m}$), and circular films were punched with a diameter of 16 mm.

Electrochemical characterizations of M(Li₂)-p-DHT (M= Mg, Zn) vs Li in liquid electrolyte

Galvanostatic cycling tests of the two active materials in liquid electrolyte were conducted vs Li in Swagelok[®]-type cells at 23° C. A Li metal disc was used as the negative electrode and fiberglass separators (Whatman[®]) were soaked with the common “LP30” battery grade electrolyte: LiPF₆ 1 M in ethylene carbonate (EC)/dimethyl carbonate (DMC) (1:1 vol./vol.) The composite positive electrodes were simply prepared in an argon environment by blending M(Li₂)-p-DHT with 33 wt.% C-ENERGY SUPER C65 using a pestle and mortar.⁴³ The average weight of these positive powder electrodes was around 5-9 mg. All cells were cycled in galvanostatic mode using a MPG-2 multichannel system (Bio-Logic SAS, Seyssinet-Pariset, France).

Electrochemical characterizations of M(Li₂)-p-DHT (M= Mg, Zn) vs Li using solid polycarbonate electrolyte

Positive electrodes made of M(Li₂)-p-DHT (M= Mg, Zn) were fabricated by making a slurry containing 70 wt.% M(Li₂)-p-DHT, 15 wt.% C65 carbon black, and 15 wt.% of a PCL-PTMC copolymer binder in acetonitrile (ACN) using a centrifugal mixer. This slurry was then uniformly coated over a carbon-coated aluminum foil, forming a positive electrode layer upon solvent evaporation. Electrode disks of diameter 12 mm were punched out using an electrode

perforator and were then thoroughly dried in a vacuum oven at 80 °C for 16 hours. The polymer electrolyte was carefully placed over the M(Li₂)-*p*-DHT electrode. For the negative electrode, a lithium metal disc with a 14 mm diameter was used. These components were assembled into pouch-type cells within an argon-filled glovebox (Figure S1). The average mass loading of electrodes was $\approx 1\text{-}2 \text{ mg cm}^{-2}$. An Arbin BT cycler was used for electrochemical measurements.

Electrochemical impedance spectroscopy measurements

EIS measurements were used to study the ionic conductivity of the polymer using the Schlumberger SI 1260 Impedance/Gain-phase Analyzer. SPEs were placed between two stainless steel blocking electrodes for this measurement. An alternating current (AC) of 10 mV was applied across a frequency spectrum ranging from 1 Hz to 10 MHz for different temperatures ranging from 25 to 100 °C. For improved interfacial contact, the cells, configured as a CR2032 coin cells, were subjected to a heating step at 90 °C for an hour. Subsequently, the cells were allowed to cool overnight before the day set for measurement.⁴⁴ Prior to each new measurement, the samples were allowed to reach a stable temperature for 30 min. Post-measurement, the data were fitted using ZView[®] software, Scribner Associates to a modified Debye circuit model for temperature below 60 °C (Figure S2) or by measuring the intercept at on the real axis of the Nyquist plot, to obtain resistance (R_b) of bulk electrolyte. The ionic conductivity was subsequently calculated using the formula $\sigma = L/(R_b \times A)$, where L represents the thickness of the polymer electrolyte film, and A is the contact area between the electrolyte and the electrode.^{41,42,45}

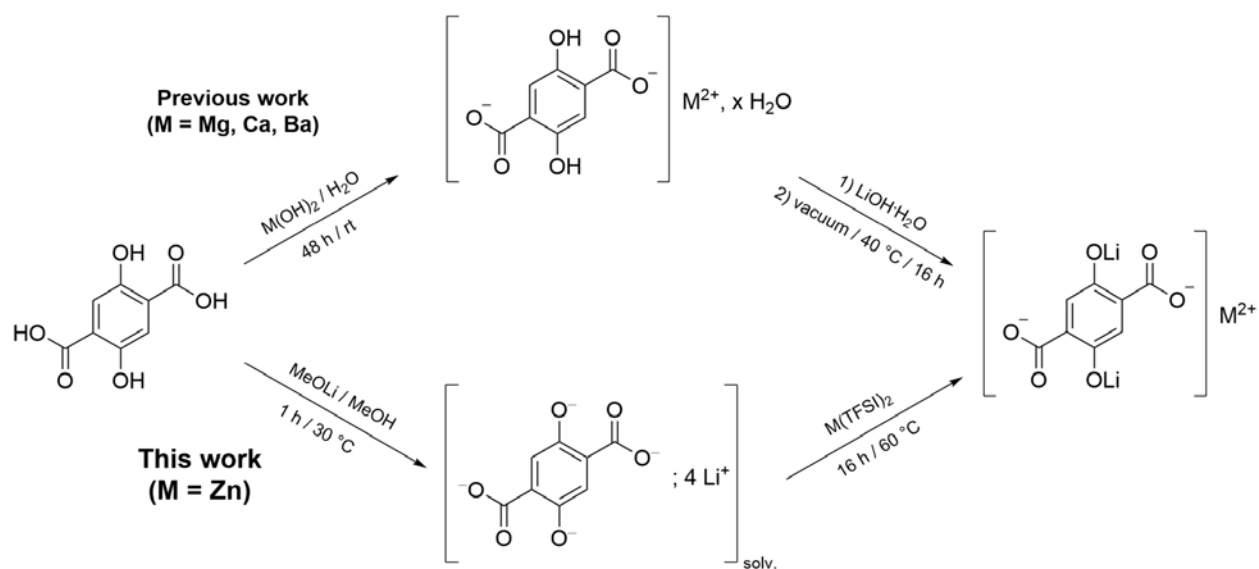
Result and Discussion

The Zn(Li₂)-p-DHT phase, chemical synthesis approach and characterizations

We have formerly developed an original chemical approach for the synthesis of a series of innovative lithiated and lamellar organic active materials based on the general formula $M_{2/n}^{n+}(\text{Li}_2)\text{-p-DHT}$ ($M^{n+} = \text{Li}^+, \text{Mg}^{2+}, \text{Ca}^{2+}, \text{and Ba}^{2+}$) and pinpointed a quasi-linear correlation between the average operating potential $\langle E \rangle$ of $M_{2/n}^{n+}(\text{Li}_2)\text{-p-DHT}$ against the ionic potential (IP) of M^{n+} ; the latter being formally a spectator cation.⁴³ Thus, the Mg^{2+} cation with its quite high IP value of 3.076 enables to reach an $\langle E \rangle$ value of ≈ 3.4 V vs Li^+/Li , which is at the state of the art for an organic lithiated insertion material.⁴⁶ Assuming an extension of this empirical correlation to (i) the 3d-block elements and (ii) an equivalent 2-D structural arrangement with the M^{n+} spectator cation (coordinated through both carboxylates and phenolates),⁴³ a similar $\langle E \rangle$ value could be anticipated with the Zn^{2+} cation due to its IP value of 2.816 (Table S1). Vlad group has indeed shown that other $p\text{-DHT}^{4-}\text{-Li}^+/\text{M}^{n+}$ coordination modes such as in the archetypal CPO-27 Metal–Organic Framework (MOF) induce quite different electrochemical properties in the solid state.⁴⁷

Our previous synthesis route to produce $\text{Mg}(\text{Li}_2)\text{-p-DHT}$ involved first the intermediate compound $\text{Mg}(\text{H}_2)\text{-p-DHT}\cdot 6\text{H}_2\text{O}$, by neutralizing the carboxylic acid groups in $\text{H}_4\text{-p-DHT}$ with $\text{Mg}(\text{OH})_{2(s)}$ in aqueous solution prior to the neutralization reaction of the hydroquinone moiety. However, the amphoteric nature and limited solubility of zinc hydroxide in water render this method ineffective for producing the $\text{Zn}(\text{Li}_2)\text{-p-DHT}$ compound. A novel, efficient, and scalable chemical synthesis method was therefore developed inspired by the chemical route reported by Chen group to obtain $\text{Li}_4\text{-p-DHT}$.⁴⁸ For the latter, 2,5-dihydroxyterephthalic acid ($\text{H}_4\text{-p-DHT}$) is

fully neutralized with MeOLi in a methanol solution leading to the precipitation of the solvate $\text{Li}_4\text{-}p\text{-DHT}\cdot\text{CH}_3\text{OH}$. However, by reproducing this chemical route, we experienced that the precipitation can be avoided through reducing the initial concentration of reactants, making a homogeneous solution of dissociated $p\text{-DHT}^{4-}/\text{Li}^+$ ions in methanol possible. Then, the simple addition of the appropriated stoichiometry of $\text{Zn}(\text{TFSI})_2$ powder induces an orange colored precipitate (Scheme 1). The precipitate was identified as non-solvated $\text{Zn}(\text{Li}_2)\text{-}p\text{-DHT}$ after drying at $130\text{ }^\circ\text{C}$ in vacuum according to TG/DSC analysis (Figure S3), FTIR measurement (Figure 1a), and both liquid $^1\text{H}/^{13}\text{C}$ NMR spectroscopy (Figure S4).



Scheme 1. Top: Synthesis route for producing $\text{M}(\text{Li}_2)\text{-}p\text{-DHT}$ ($\text{M} = \text{Mg}, \text{Ca}, \text{and Ba}$);⁴³ Down: Novel synthesis route to selectively prepare $\text{Zn}(\text{Li}_2)\text{-}p\text{-DHT}$ from solvated $p\text{-DHT}^{4-}/\text{Li}^+$ ions in MeOH.

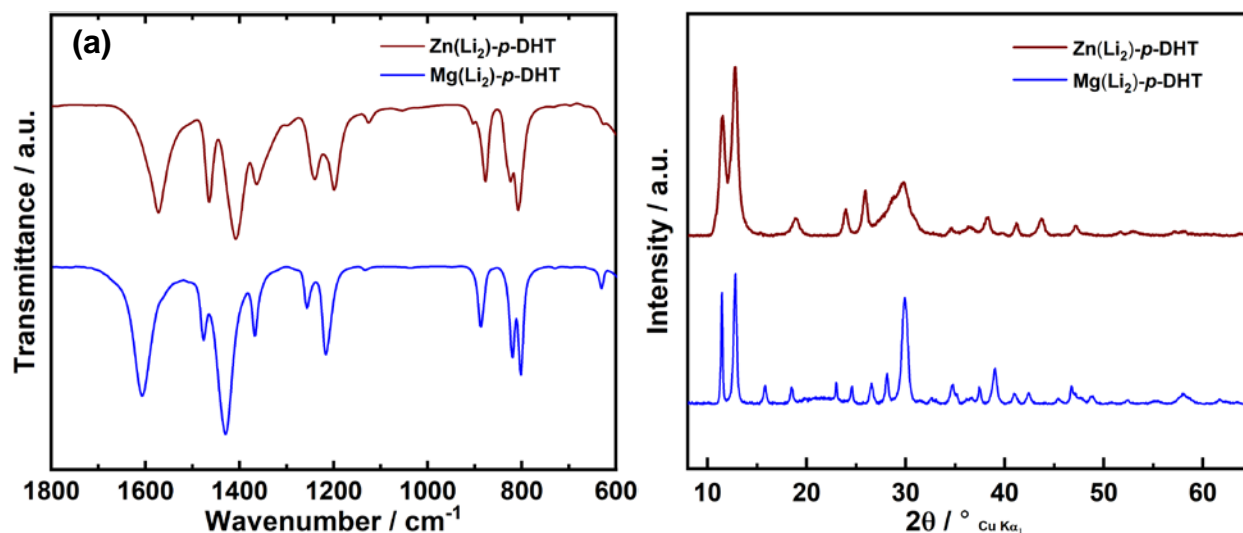


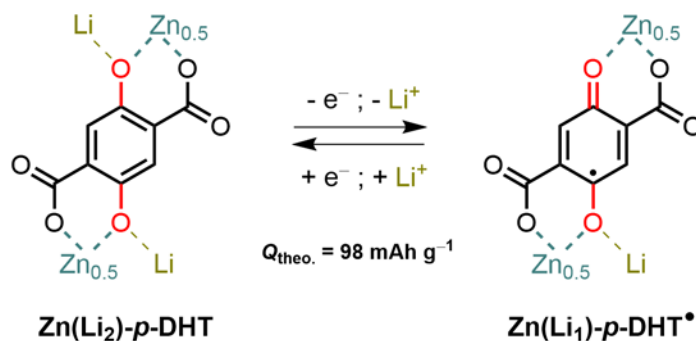
Figure 1. (a) Overlaid FTIR spectra (a) and X-Ray powder diffraction patterns (b) of Zn(Li₂)-p-DHT (brown) and Mg(Li₂)-p-DHT (blue).

Interestingly, the FTIR spectra analysis reveals that both Zn(Li₂)-p-DHT and Mg(Li₂)-p-DHT share identical vibration peaks including the fingerprint region, which indicates a quite similar 2-D structural arrangement in the solid state. This observation was further confirmed by PXRD (Figure 1b) since the two crystalline phases display matching peak positions with, however, a noticeable broadening of the diffraction peaks for Zn(Li₂)-p-DHT suggesting a less crystalline phase for this salt. Finally, the Zn and Li contents measured by ICP-AES elemental analyses confirmed the expected stoichiometry for Zn(Li₂)-p-DHT (Figure S5).

Comparison of electrochemical cycling performance of M(Li₂)-p-DHT (M = Zn, Mg) vs Li in conventional liquid electrolyte

Electrochemical investigations vs Li were performed in Swagelok[®]-type cells, according to a procedure similar to the one previously reported for Mg(Li₂)-p-DHT using LiPF₆ 1 M in

EC/DMC (LP30) by scanning the potential range 2.4–4 V vs Li⁺/Li, at a cycling rate corresponding to one Li⁺ exchanged per Zn(Li₂)-*p*-DHT in 5 h.⁴³ Scheme 2 shows the expected electrochemical reaction limited to half of the theoretical value since the fully oxidized quinone form was never observed in all our former experimental studies on lithiated DHT-based electrode materials.^{8,9,43,49,50} The explanation will be reported in an upcoming paper.



Scheme 2. Expected delithiation/lithiation process at the molecular level for Zn(Li₂)-*p*-DHT based on a reversible one-electron reaction giving rise to the semi-quinone radical form.

Figure 2 compares the typical galvanostatic charging–discharging profile related to Zn(Li₂)-*p*-DHT with former data recorded in similar experimental conditions for the Mg counterpart phase. In short, the electrochemical behavior for Zn(Li₂)-*p*-DHT pointed out an efficient reversible delithiation/lithiation process but also an average working potential located at ≈3.4 V vs Li⁺/Li, as anticipated based on the IP value of Zn²⁺ and considering an equivalent 2-D structural arrangement between both Mg and Zn phases. The similarities and differences of the two cycling curve profiles can also be visualized by plotting the differential capacity curves and the normalized potential-capacity traces (Figure S6). While the magnesium compound reveals a two-phase region from Mg(Li₂)-*p*-DHT to Mg(Li_{1.4})-*p*-DHT, the cycling curve for Zn(Li₂)-*p*-DHT appears featureless compatible with a solid solution process. As also expected, the related

coulometric measurements confirms that the reversible capacity is still limited to one-electron reaction; the Kolbe decarboxylation reaction occurring beyond 4.1 V vs Li⁺/Li. This new lithiated insertion material achieved an initial specific charge capacity of 85 mA h g⁻¹ close to the theoretical specific capacity (*i.e.*, 98 mA h g⁻¹ based on one-electron exchange per *p*-DHT moiety). There was a slight decrease in terms of capacity retention upon cycling (64.3 mA h g⁻¹ after 50 cycles) as shown in Figure 2b. In comparison, Mg(Li₂)-*p*-DHT demonstrated a capacity retention of 99.9% after 50 cycles (Figure 2c-d). A simple explanation could be related to the ionic-covalent character of the M–O bond. As the size of the cation decreases, its polarizing power increases and the covalent contribution becomes more significant. Consequently, the covalent contribution in the Mg–O bond is higher than in the Zn–O bond giving rise to a better stability of the Mg(Li₂)-*p*-DHT network. Additional electrochemical measurements were then performed on the Zn(Li₂)-*p*-DHT compound at 0 °C and 45 °C (Figure S7). Although the same electrochemical profile was found at these two temperatures, only 70 mA h g⁻¹ were recorded after the first charge at 0 °C but paired with good stability upon cycling. This behavior is quite common and simply reflects kinetic limitations in electrode operation. At 45 °C, the active material delivers a capacity in charge slightly exceeding the theoretical capacity while showing low cycling stability and poor coulombic efficiency. This feature can be attributed to parasitic reactions and probably to a certain thermal sensitivity of this active material.

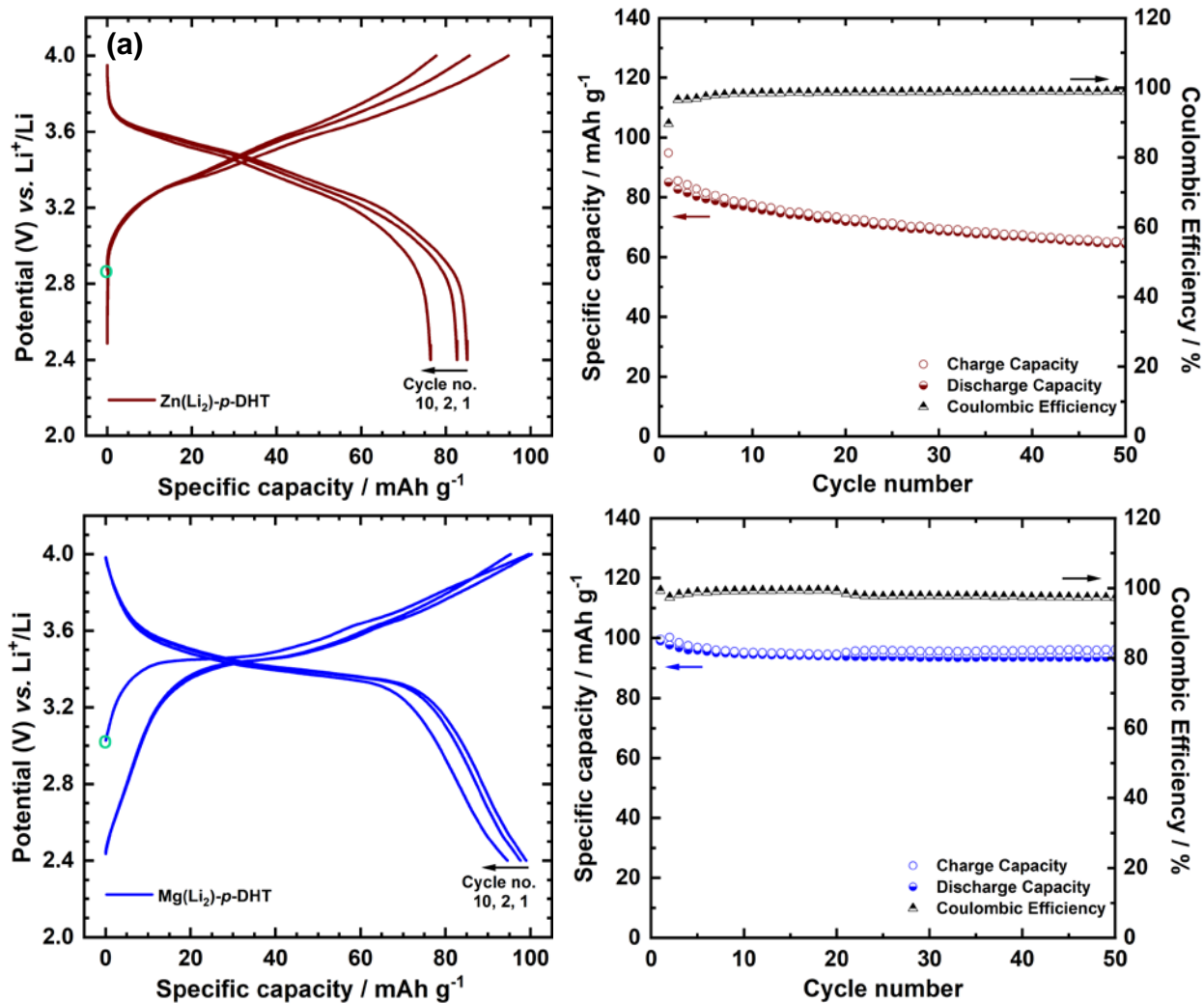


Figure 2. Charge/discharge electrochemical performance of M(Li₂)-p-DHT (M = Zn, Mg) electrode material vs Li, galvanostatically cycled in LiPF₆ 1 M in EC/DMC at a rate of 1 Li⁺/5 h. (a) Potential vs specific capacity curve (cycle no. 1, 2, 10) using Zn(Li₂)-p-DHT as the active electrode material; the green circle indicates the starting potential and (b) corresponding capacity retention curve of Zn(Li₂)-p-DHT. (c) Potential vs specific capacity curve (cycle no. 1, 2, 10) using Mg(Li₂)-p-DHT as the active electrode material and (d) corresponding capacity retention curve from ref. ⁴³.

Last but not least, it was possible to update our former correlation based on both FTIR and electrochemical data,⁴³ by the addition of Zn(Li₂)-*p*-DHT as a new material example (Figure 3). For the sake of comparison, Figure 3a summarizes first the representative FTIR spectra of M_{2/n}ⁿ⁺(Li₂)-*p*-DHT (Mⁿ⁺ = Li⁺, Mg²⁺, Ca²⁺, Ba²⁺, and Zn²⁺) focused on the fingerprint region, which highlights the most obvious band shifts depending on Mⁿ⁺. As previously reported,⁴³ the average position of the ν_{as}(COO⁻) band was particularly monitored because the latter is known to be sensitive to the electron density on the carboxylate carbon; its shift to higher wavenumbers is correlated to an electron density decrease.⁵¹ The shift of the ν(CO–Li) vibration band could also be used⁵² since Mⁿ⁺ is supposed to be coordinated through both carboxylates and phenolates. Figure 3b shows this updated correlation demonstrating the Zn phase belongs to the quasi-linear trend previously found when plotting both ν_{as}(COO⁻) and <E> against the IP value of Mⁿ⁺.

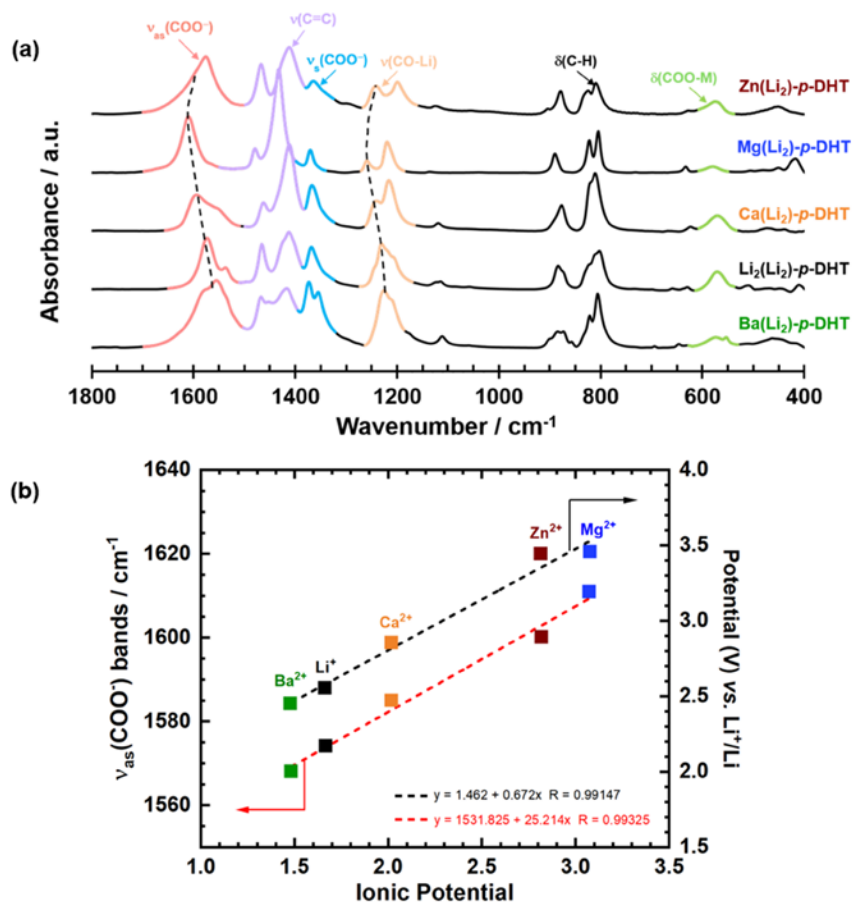


Figure 3. (a) Overlaid FTIR spectra of $M_{2/n}^{n+}(\text{Li}_2)\text{-}p\text{-DHT}$ ($M^{n+} = \text{Li}^+, \text{Mg}^{2+}, \text{Ca}^{2+}, \text{Ba}^{2+}$, and Zn^{2+}) focused on the fingerprint region showing close similarities of bending vibrations within this family of lamellar organic materials and obvious shifts depending on the spectator cation M^{n+} within the structure. Note that $\nu_{\text{as}}(\text{COO}^-)$ involving multiple vibration bands, the dotted line shows the average trend. (b) Correlation between the asymmetric vibration mode of the carboxylate functional group ($\nu_{\text{as}}(\text{COO}^-)$) and the average operating potential related to one Li^+ extraction/insertion for this series of materials.

PCL-PTMC as the electrolyte, synthesis and characterizations

It has formerly been reported that SPEs composed of an 80:20 PCL-PTMC copolymer ratio, with a LiTFSI salt concentration of 28 wt.% or higher, demonstrate optimal ionic conductivity without compromising mechanical characteristics.^{42,53} Hence, we selected this specific polymer composition for all our experiments. The TGA traces of PCL-PTMC polymer with and without LiTFSI salt are given in the Figure 4a. This polymer electrolyte is very stable up to ≈ 200 °C. The the plateau at around 360–410 °C, roughly proportional to the amount of salt in the electrolyte sample, is as expected absent in the curve of polymer without salt.⁵⁴ Figure S8 shows a DSC curve of PCL:PTMC polymer with 28 wt% LiTFSI salt, indicating a sufficiently low T_g value of -38 °C. Electrochemical impedance spectroscopy studies of the polymer electrolyte was conducted at different temperatures to understand the temperature dependence of ionic conductivity of the polymer electrolyte, and the corresponding Nyquist plot and conductivity plots are given in Figure 4b-c, respectively. In the Nyquist plot, the disappearance of the semi-circle is observed at 60 °C. At a temperature greater than or equal to 60 °C, the impedance showed purely resistive behavior. The FTIR spectrum of the polymer electrolyte (Figure 4d) with and without LiTFSI shows a similar trend as in previously reported literature^{53,55} and exhibits characteristic peaks of the PCL-PTMC co-polymer with the LiTFSI salt (Figure S9).⁵⁵

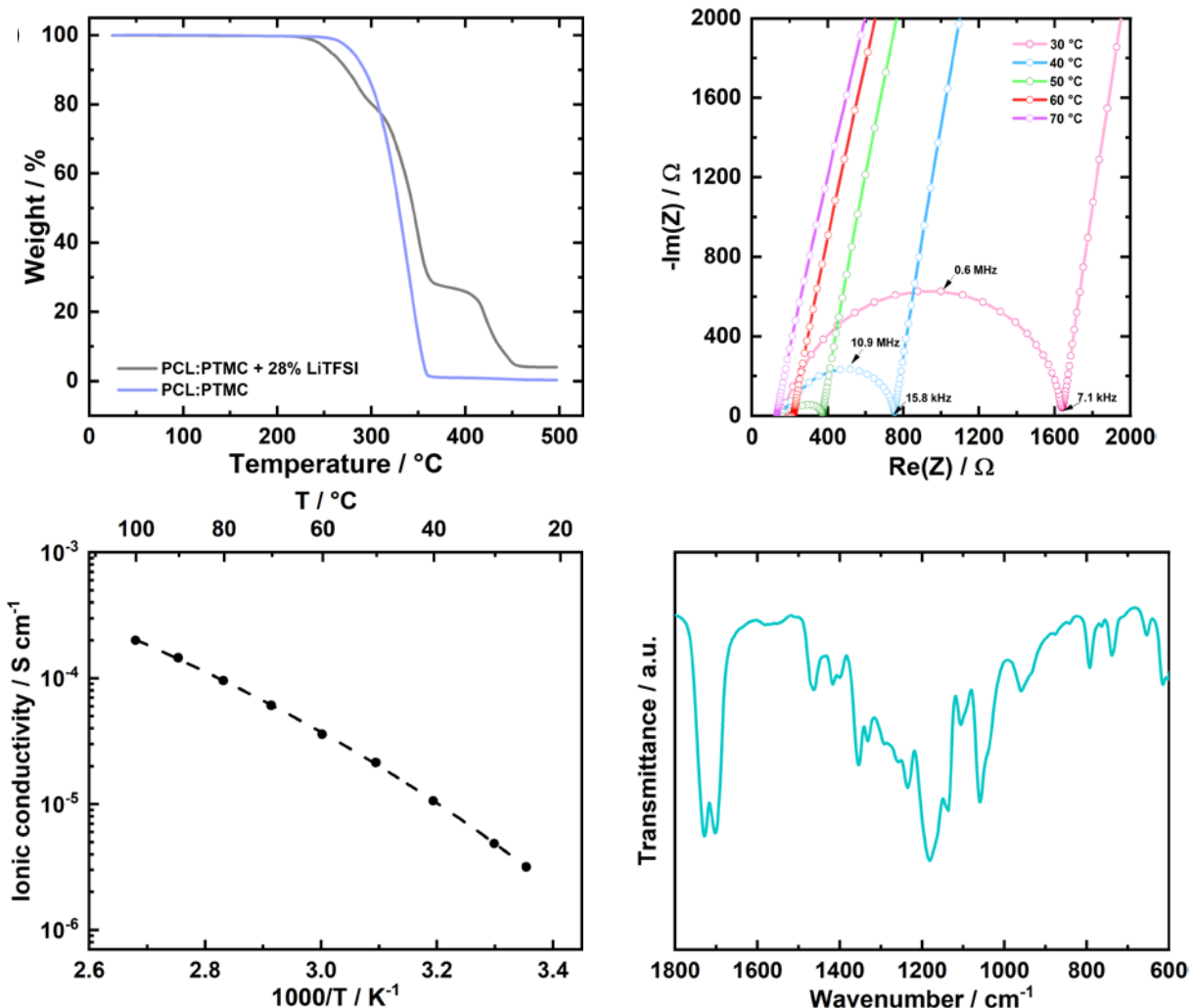


Figure 4. (a) TGA traces of PCL-PTMC polymer with and without LiTFSI salt performed under nitrogen atmosphere at a heating rate of 10 °C.min⁻¹ (b) Nyquist plots of PCL-PTMC: LiTFSI SPE at different temperatures (c) Ionic conductivity vs temperature plot with Vogel–Fulcher–Tammann (VFT) fitting shown as dotted lines (d) FTIR spectra of PCL-PTMC: LiTFSI SPE.

Comparison of the electrochemical cycling performance of $M(Li_2)$ -p-DHT ($M = Zn, Mg$) vs Li in solid polyester-polycarbonate electrolyte

For the electrode formulation used for testing with PCL-PTMC: LiTFSI polymer electrolyte, we employed the very same PCL-PTMC polymer as an electrode binder too, expecting an enhanced interfacial contact and a continuity in ionic conduction throughout the volume of the electrode. This approach aims to compensate the challenges posed by the inherent rigidity of solid electrolytes when infiltrating the porous structures in the electrode. Figure S10a displays a SEM cross-sectional view of the as-obtained composite electrodes designed for the testing with SPE. Figure S11b reveals the intricate network of polymer filaments enveloping the entirety of active material and carbon black. Following an extensive series of electrochemical testing across various temperatures and subsequent analysis of conductivity data for the PCL-PTMC SPE, we identified 60 °C as the optimal operational temperature for the Li | PCL-PTMC:LiTFSI | M(Li₂)-*p*-DHT assembly. At this temperature, the ionic conductivity is sufficient for the cycling rate employed and the polymer is soft enough to ensure good interfacial compatibility with the electrodes. At the same time, it still possessed the mechanical properties at 60 °C to separate the electrodes without the employment of any external separator. All cells were subjected to a rest period at 60 °C prior to cycling to enhance the contact at interface; effect of this pre-conditioning step is demonstrated in Figure S11. Finally, such activated cells were also cycled at different temperatures. Figure S12 depicts the potential vs specific capacity curve for Li | PCL-PTMC:LiTFSI | Mg(Li₂)-*p*-DHT pouch cells cycle at 25 °C, 40 °C, 60 °C, and 80 °C, respectively. We observed that when the cells are cycled at 25 °C, we obtained stable cycling but the significant polarization is limiting the cell to reach its maximum achievable specific capacity, primarily due to the lower ionic conductivity of the polymer electrolyte at this temperature (Figure 4c) which is evident from the EIS data, also inadequate contact at the electrode-electrolyte interface contributes to this problem. As anticipated, a reduction in polarization was

observed at 40 °C, but yet a considerable degree of polarization persisted, leading to a low specific capacity. At a temperature of 80 °C, in turn, a more significant fading in capacity is evident, where the capacity after 10 cycles falls below that observed at 60 °C. This may be due to undesirable side reactions that are more prevalent at higher temperatures as also observed in liquid electrolyte medium (Figure S7b), or that the polymer is too soft to withstand formation of dendrites or mossy lithium at the anode. At 60 °C, the characteristics of the charge-discharge curve almost matches those of a cell tested in regular liquid electrolyte (LP30).

Mirroring the electrochemical performance observed with liquid electrolytes, the Mg(Li₂)-*p*-DHT exhibits an initial specific discharge capacity of ≈ 99 mAh g⁻¹ and an average operating potential of ≈ 3.4 V vs Li⁺/Li (Figure 5a), with a decent capacity retention over 50 cycles for this unoptimized first electrochemical testing (Figure 5b). This highlights the excellent compatibility between a terephthalate-based OEM and a SPE in a soft solid-state system. Similarly, the charge-discharge profile of Zn(Li₂)-*p*-DHT in SPE mirrors its performance in liquid electrolyte, both displaying an initial specific discharge capacity ≈ 85 mAh g⁻¹ and an average operating potential of ≈ 3.4 V vs Li (Figure 5c). However, in contrast to Mg(Li₂)-*p*-DHT, Zn(Li₂)-*p*-DHT shows pronounced capacity fading in PCL-PTMC: LiTFSI polymer electrolyte (Figure 5d). Further studies is essential to elucidate the reasons for this problem.

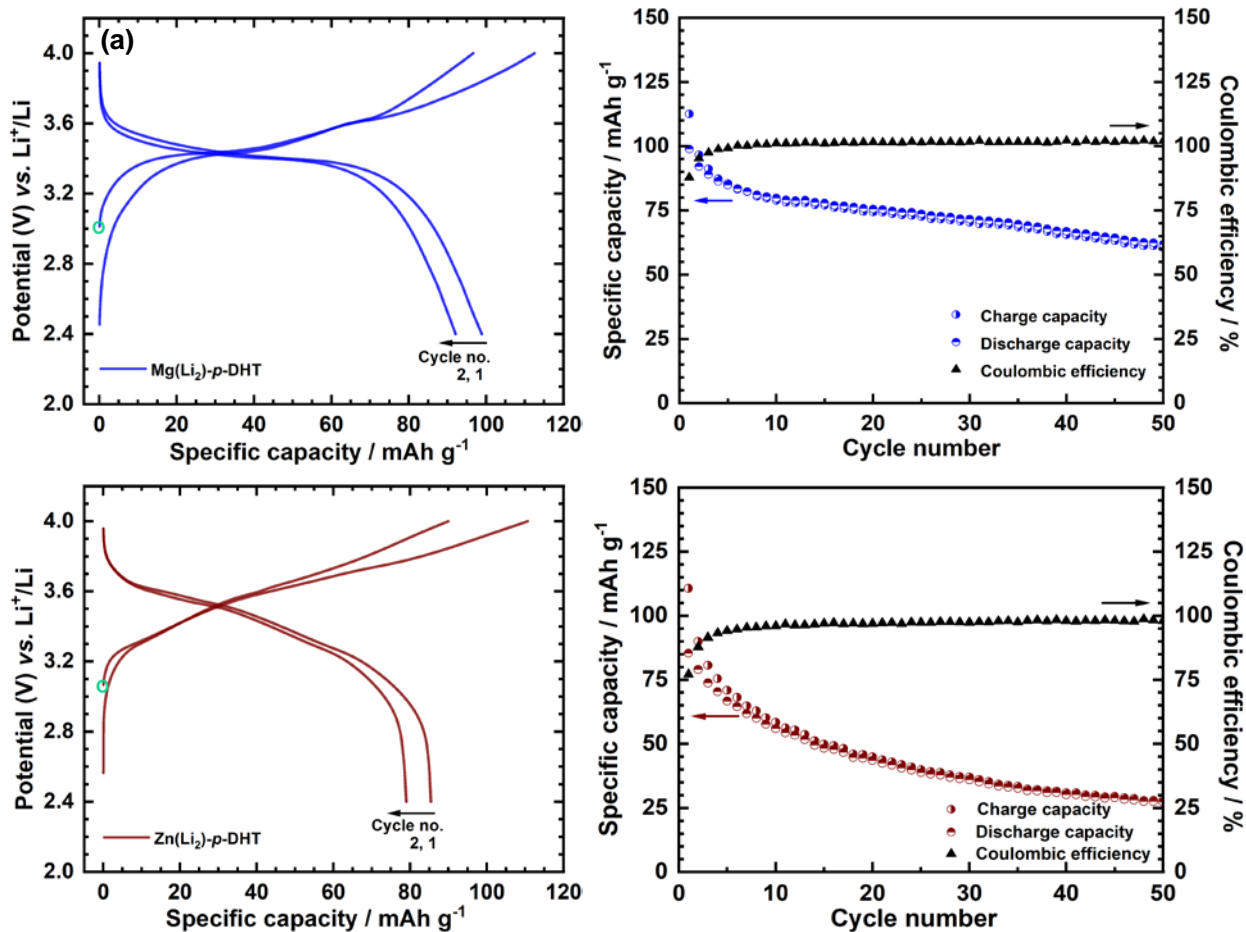


Figure 5. Electrochemical charge/discharge performance of M(Li₂)-p-DHT (M = Zn, Mg) electrode materials vs Li, galvanostatically cycled in PCL-PTMC:LiTFSI SPE at a rate of 1 Li⁺/10 h; at an operating temperature of 60 °C. (a) Potential vs specific capacity curve (cycle no. 1, 2) using Mg(Li₂)-p-DHT as the active electrode material; the green circle indicates the starting potential. (b) Corresponding capacity retention curve of Mg(Li₂)-p-DHT. (c) Potential vs specific capacity curve (cycle no. 1, 2) using Zn(Li₂)-p-DHT as the active electrode material; the green circle indicates the starting potential and (d) corresponding capacity retention curve of Zn(Li₂)-p-DHT.

Conclusions

In this study, we report the successful development of a new organic positive electrode material, Zn(Li₂)-*p*-DHT, through a novel, scalable synthesis approach and its compatibility with a solid polymer electrolyte. The synthesis of the active material was motivated by the high IP of Zn²⁺ similar to that of Mg²⁺ by taking into account our recent empirical correlation between the average operating potential of lamellar M_{2/n}ⁿ⁺(Li₂)-*p*-DHT insertion materials vs the IP value of Mⁿ⁺. This electrode material demonstrated an initial specific capacity of 85 mAh g⁻¹ (theoretical capacity ≈ 98 mAh g⁻¹) when tested in a standard LP30 liquid electrolyte, with a notable capacity retention and high coulombic efficiency of 98.9%. Furthermore, the compatibility of Zn(Li₂)-*p*-DHT, as well as the previously reported Mg(Li₂)-*p*-DHT, with SPE (PCL-PTMC co-polymer) was investigated, representing a pioneering advancement in the realm of Li-organic soft solid-state battery systems, opening new avenues for the development of advanced energy storage systems that are cheaper, safer and more sustainable. While this SPE has shown to be functional with inorganic cathodes at room temperature, operational temperatures of 60 °C were here necessary for useful cell performance, which can be hypothesized to origin from resistances in the interface between the organic electrode and the SPE. This could potentially be engineered in the future.

Our findings indicate that both Zn(Li₂)-*p*-DHT and Mg(Li₂)-*p*-DHT exhibit identical electrochemical behaviors in conventional liquid electrolyte and SPE, under the optimal operational temperature of 60 °C. This behavior shows the potential of this combination of materials to function as the foundation for a new class of electrochemical energy storage solutions.

Notably, Zn(Li₂)-*p*-DHT has shown promising capacity retention over 50 cycles in liquid LP30 electrolyte. In contrast, the Zn(Li₂)-*p*-DHT electrodes have large capacity loss in SPE, suggesting the need for further in-depth studies to understand and overcome this limitation. In conclusion, this work opens a novel and effective solution for the developing safer, more sustainable electrochemical energy storage systems.

ASSOCIATED CONTENT

Supporting Information

The Supporting Information is available free of charge at <https://pubs.acs.org/doi/XXX>.

Supporting figures and tables including relevant ^1H and ^{13}C spectra and Zn quantification measured by ICP-AES (PDF).

AUTHOR INFORMATION

Corresponding Author

*Philippe Poizot – Nantes Université, CNRS, Institut des Matériaux de Nantes Jean Rouxel, IMN, F-44000 Nantes, France; ORCID ID: 0000-0003-1865-4902; Email: philippe.poizot@cnrsmn.fr

Authors

Aswadh Shyma Sajeevan – Nantes Université, CNRS, Institut des Matériaux de Nantes Jean Rouxel, IMN, F-44000 Nantes, France; ORCID ID: 0009-0008-2959-3993

Lou Bernard – Nantes Université, CNRS, Institut des Matériaux de Nantes Jean Rouxel, IMN, F-44000 Nantes, France

Pierre Tran-Van – Technocentre Renault, 1 Avenue du Golf, 78280 Guyancourt, France; ORCID ID: 0000-0003-2743-9737

Daniel Brandell – Department of Chemistry–Ångström Laboratory, Uppsala University, SE-751 21 Uppsala, Sweden; ORCID ID: 0000-0002-8019-2801

Stéven Renault– Nantes Université, CNRS, Institut des Matériaux de Nantes Jean Rouxel, IMN, F-44000 Nantes, France; ORCID ID: 0000-0002-6500-0015

Author Contributions

The manuscript was written through contributions of all authors. All authors have given approval to the final version of the manuscript.

Funding Sources

National Agency for Research and Technology (ANRT) CIFRE n° 2018/1264; Marie Skłodowska-Curie grant agreement #945357 (DESTINY COFUND PhD Program); The Swedish Research Council (Grant No. 2018-04506); 04506); The European Research Council (ERC), Grant No. 771777 FUN POLYSTORE.

ACKNOWLEDGMENT

L.B., P.T.-V., S.R., and P.P. acknowledge the support by the National Agency for Research and Technology (ANRT) through an Industrial Research Convention (CIFRE) between IMN/CNRS UMR 6502 and RENAULT group (CIFRE n° 2018/1264). As a part of the DESTINY PhD programme, this publication is acknowledged by funding from the European Union's Horizon2020 research and innovation programme under the Marie Skłodowska-Curie Actions COFUND (Grant Agreement #945357)". D.B. acknowledges support from the Swedish Research Council and STandUP for Energy and the European Research Council (ERC). A.S.S. deeply thanks I. L. Johansson, J. Mindemark, A. Oltean, Z. J. R. Ashworth, K. Elbouazzaoui, T. Patranika from UU for fruitful discussions and guidance as well as M. Nicolas (NU) for his help in the synthesis of Mg(Li₂)-*p*-DHT. This work includes NMR experiments carried out on the

CEISAM NMR platform, Nantes Université. Both Li and Zn contents were determined by ICP-AES analyses performed at the LPG-UMR 6112 (C. La, M. Rivoal), Nantes Université.

References

- (1) Goodenough, J. B. Electrochemical Energy Storage in a Sustainable Modern Society. *Energy Environ. Sci.* **2014**, *7* (1), 14–18. <https://doi.org/10.1039/C3EE42613K>.
- (2) Kim, T.; Park, J.; Chang, S. K.; Choi, S.; Ryu, J. H.; Song, H. The Current Move of Lithium Ion Batteries Towards the Next Phase. *Adv. Energy Mater.* **2012**, *2* (7), 860–872. <https://doi.org/10.1002/aenm.201200028>.
- (3) Poizot, P.; Dolhem, F. Clean Energy New Deal for a Sustainable World: From Non-CO₂ Generating Energy Sources to Greener Electrochemical Storage Devices. *Energy Environ. Sci.* **2011**, *4* (6), 2003. <https://doi.org/10.1039/c0ee00731e>.
- (4) Duarte Castro, F.; Vaccari, M.; Cutaia, L. Valorization of Resources from End-of-Life Lithium-Ion Batteries: A Review. *Crit. Rev. Environ. Sci. Technol.* **2022**, *52* (12), 2060–2103. <https://doi.org/10.1080/10643389.2021.1874854>.
- (5) Poizot, P.; Gaubicher, J.; Renault, S.; Dubois, L.; Liang, Y.; Yao, Y. Opportunities and Challenges for Organic Electrodes in Electrochemical Energy Storage. *Chem. Rev.* **2020**, *120* (14), 6490–6557. <https://doi.org/10.1021/acs.chemrev.9b00482>.
- (6) Xu, J.; Cai, X.; Cai, S.; Shao, Y.; Hu, C.; Lu, S.; Ding, S. HIGH-ENERGY Lithium-Ion Batteries: Recent Progress and a Promising Future in Applications. *ENERGY Environ. Mater.* **2023**, *6* (5), e12450. <https://doi.org/10.1002/eem2.12450>.
- (7) Chen, H.; Armand, M.; Demailly, G.; Dolhem, F.; Poizot, P.; Tarascon, J. From Biomass to a Renewable Li_xC₆O₆ Organic Electrode for Sustainable Li-Ion Batteries. *ChemSusChem* **2008**, *1* (4), 348–355. <https://doi.org/10.1002/cssc.200700161>.
- (8) Renault, S.; Gottis, S.; Barrès, A.-L.; Courty, M.; Chauvet, O.; Dolhem, F.; Poizot, P. A Green Li–Organic Battery Working as a Fuel Cell in Case of Emergency. *Energy Environ. Sci.* **2013**, *6* (7), 2124. <https://doi.org/10.1039/c3ee40878g>.
- (9) Gottis, S.; Barrès, A.-L.; Dolhem, F.; Poizot, P. Voltage Gain in Lithiated Enolate-Based Organic Cathode Materials by Isomeric Effect. *ACS Appl. Mater. Interfaces* **2014**, *6* (14), 10870–10876. <https://doi.org/10.1021/am405470p>.
- (10) Miroshnikov, M.; Divya, K. P.; Babu, G.; Meiyazhagan, A.; Reddy Arava, L. M.; Ajayan, P. M.; John, G. Power from Nature: Designing Green Battery Materials from Electroactive Quinone Derivatives and Organic Polymers. *J. Mater. Chem. A* **2016**, *4* (32), 12370–12386. <https://doi.org/10.1039/C6TA03166H>.
- (11) Lee, B.; Ko, Y.; Kwon, G.; Lee, S.; Ku, K.; Kim, J.; Kang, K. Exploiting Biological Systems: Toward Eco-Friendly and High-Efficiency Rechargeable Batteries. *Joule* **2018**, *2* (1), 61–75. <https://doi.org/10.1016/j.joule.2017.10.013>.
- (12) Navalpotro, P.; Castillo-Martínez, E.; Carretero-González, J. Sustainable Materials for Off-Grid Battery Applications: Advances, Challenges and Prospects. *Sustain. Energy Fuels* **2021**, *5* (2), 310–331. <https://doi.org/10.1039/D0SE01338B>.
- (13) Nguyen, T. P.; Easley, A. D.; Kang, N.; Khan, S.; Lim, S.-M.; Rezenom, Y. H.; Wang, S.; Tran, D. K.; Fan, J.; Letteri, R. A.; He, X.; Su, L.; Yu, C.-H.; Lutkenhaus, J. L.; Wooley, K. L. Polypeptide Organic Radical Batteries. *Nature* **2021**, *593* (7857), 61–66. <https://doi.org/10.1038/s41586-021-03399-1>.

- (14) An, S. Y.; Schon, T. B.; McAllister, B. T.; Seferos, D. S. Design Strategies for Organic Carbonyl Materials for Energy Storage: Small Molecules, Oligomers, Polymers and Supramolecular Structures. *EcoMat* **2020**, *2* (4), e12055. <https://doi.org/10.1002/eom2.12055>.
- (15) Esser, B.; Dolhem, F.; Becuwe, M.; Poizot, P.; Vlad, A.; Brandell, D. A Perspective on Organic Electrode Materials and Technologies for next Generation Batteries. *J. Power Sources* **2021**, *482*, 228814. <https://doi.org/10.1016/j.jpowsour.2020.228814>.
- (16) Lu, Y.; Chen, J. Prospects of Organic Electrode Materials for Practical Lithium Batteries. *Nat. Rev. Chem.* **2020**, *4* (3), 127–142. <https://doi.org/10.1038/s41570-020-0160-9>.
- (17) Lakraychi, A. E.; Dolhem, F.; Vlad, A.; Becuwe, M. Organic Negative Electrode Materials for Metal-Ion and Molecular-Ion Batteries: Progress and Challenges from a Molecular Engineering Perspective. *Adv. Energy Mater.* **2021**, *11* (32), 2101562. <https://doi.org/10.1002/aenm.202101562>.
- (18) Xie, Y.; Zhang, K.; Yamauchi, Y.; Oyaizu, K.; Jia, Z. Nitroxide Radical Polymers for Emerging Plastic Energy Storage and Organic Electronics: Fundamentals, Materials, and Applications. *Mater. Horiz.* **2021**, *8* (3), 803–829. <https://doi.org/10.1039/D0MH01391A>.
- (19) Goujon, N.; Casado, N.; Patil, N.; Marcilla, R.; Mecerreyes, D. Organic Batteries Based on Just Redox Polymers. *Prog. Polym. Sci.* **2021**, *122*, 101449. <https://doi.org/10.1016/j.progpolymsci.2021.101449>.
- (20) Zhao, L.; Lakraychi, A. E.; Chen, Z.; Liang, Y.; Yao, Y. Roadmap of Solid-State Lithium–Organic Batteries toward 500 Wh kg⁻¹. *ACS Energy Lett.* **2021**, *6* (9), 3287–3306. <https://doi.org/10.1021/acseenergylett.1c01368>.
- (21) Kye, H.; Kang, Y.; Jang, D.; Kwon, J. E.; Kim, B.-G. p-Type Redox-Active Organic Electrode Materials for Next-Generation Rechargeable Batteries. *Adv. Energy Sustain. Res.* **2022**, *3* (8), 2200030. <https://doi.org/10.1002/aesr.202200030>.
- (22) Saal, A.; Hagemann, T.; Schubert, U. S. Polymers for Battery Applications—Active Materials, Membranes, and Binders. *Adv. Energy Mater.* **2021**, *11* (43), 2001984. <https://doi.org/10.1002/aenm.202001984>.
- (23) Yang, G.; Zhu, Y.; Hao, Z.; Lu, Y.; Zhao, Q.; Zhang, K.; Chen, J. Organic Electroactive Materials for Aqueous Redox Flow Batteries. *Adv. Mater.* **2023**, *35* (33), 2301898. <https://doi.org/10.1002/adma.202301898>.
- (24) Xie, J.; Zhang, Q. Recent Progress in Aqueous Monovalent-Ion Batteries with Organic Materials as Promising Electrodes. *Mater. Today Energy* **2020**, *18*, 100547. <https://doi.org/10.1016/j.mtener.2020.100547>.
- (25) Brandell, D.; Mindemark, J.; Hernández, G. *Polymer-Based Solid State Batteries*; Walter de Gruyter GmbH & Co KG, 2021.
- (26) Xu, W.; Wang, J.; Ding, F.; Chen, X.; Nasybulin, E.; Zhang, Y.; Zhang, J.-G. Lithium Metal Anodes for Rechargeable Batteries. *Energy Env. Sci* **2014**, *7* (2), 513–537. <https://doi.org/10.1039/C3EE40795K>.
- (27) Armand, M.; Chabagno, J. M.; Duclot, M. J. *Second international meeting on solid electrolytes, University of St Andrews, Scotland, September 20-22, 1978* | WorldCat.org. <https://search.worldcat.org/title/230397846> (accessed 2024-02-01).
- (28) Gorecki, W.; Jeannin, M.; Belorizky, E.; Roux, C.; Armand, M. Physical Properties of Solid Polymer Electrolyte PEO(LiTFSI) Complexes. *J. Phys. Condens. Matter* **1995**, *7* (34), 6823–6832. <https://doi.org/10.1088/0953-8984/7/34/007>.

- (29) Lascaud, S.; Perrier, M.; Vallee, A.; Besner, S.; Prud'homme, J.; Armand, M. Phase Diagrams and Conductivity Behavior of Poly(Ethylene Oxide)-Molten Salt Rubbery Electrolytes. *Macromolecules* **1994**, *27* (25), 7469–7477. <https://doi.org/10.1021/ma00103a034>.
- (30) Armand, M. The History of Polymer Electrolytes. *Solid State Ion.* **1994**, *69* (3–4), 309–319. [https://doi.org/10.1016/0167-2738\(94\)90419-7](https://doi.org/10.1016/0167-2738(94)90419-7).
- (31) Shanmukaraj, D.; Ranque, P.; Ben Youcef, H.; Rojo, T.; Poizot, P.; Grugeon, S.; Laruelle, S.; Guyomard, D. Review—Towards Efficient Energy Storage Materials: Lithium Intercalation/Organic Electrodes to Polymer Electrolytes—A Road Map (Tribute to Michel Armand). *J. Electrochem. Soc.* **2020**, *167* (7), 070530. <https://doi.org/10.1149/1945-7111/ab787a>.
- (32) Mindemark, J.; Lacey, M. J.; Bowden, T.; Brandell, D. Beyond PEO—Alternative Host Materials for Li⁺-Conducting Solid Polymer Electrolytes. *Prog. Polym. Sci.* **2018**, *81*, 114–143. <https://doi.org/10.1016/j.progpolymsci.2017.12.004>.
- (33) Berthier, C.; Gorecki, W.; Minier, M.; Armand, M. B.; Chabagno, J. M.; Rigaud, P. Microscopic Investigation of Ionic Conductivity in Alkali Metal Salts-Poly(Ethylene Oxide) Adducts. *Solid State Ion.* **1983**, *11* (1), 91–95. [https://doi.org/10.1016/0167-2738\(83\)90068-1](https://doi.org/10.1016/0167-2738(83)90068-1).
- (34) Rupp, B.; Schmuck, M.; Balducci, A.; Winter, M.; Kern, W. Polymer Electrolyte for Lithium Batteries Based on Photochemically Crosslinked Poly(Ethylene Oxide) and Ionic Liquid. *Eur. Polym. J.* **2008**, *44* (9), 2986–2990. <https://doi.org/10.1016/j.eurpolymj.2008.06.022>.
- (35) Croce, F.; Appetecchi, G. B.; Persi, L.; Scrosati, B. Nanocomposite Polymer Electrolytes for Lithium Batteries. *Nature* **1998**, *394* (6692), 456–458. <https://doi.org/10.1038/28818>.
- (36) Le Nest, J. F.; Gandini, A.; Cheradame, H.; Cohen-Addad, J. P. Influence of Lithium Perchlorate on the Properties of Polyether Networks: Specific Volume and Glass Transition Temperature. *Macromolecules* **1988**, *21* (4), 1117–1120. <https://doi.org/10.1021/ma00182a044>.
- (37) Homann, G.; Stolz, L.; Nair, J.; Laskovic, I. C.; Winter, M.; Kasnatscheew, J. Poly(Ethylene Oxide)-Based Electrolyte for Solid-State-Lithium-Batteries with High Voltage Positive Electrodes: Evaluating the Role of Electrolyte Oxidation in Rapid Cell Failure. *Sci. Rep.* **2020**, *10* (1), 4390. <https://doi.org/10.1038/s41598-020-61373-9>.
- (38) Perumal, P.; Christopher Selvin, P.; Selvasekarapandian, S.; Sivaraj, P.; Abhilash, K. P.; Moniha, V.; Manjula Devi, R. Plasticizer Incorporated, Novel Eco-Friendly Bio-Polymer Based Solid Bio-Membrane for Electrochemical Clean Energy Applications. *Polym. Degrad. Stab.* **2019**, *159*, 43–53. <https://doi.org/10.1016/j.polymdegradstab.2018.11.013>.
- (39) Lécuyer, M.; Gaubicher, J.; Barrès, A.-L.; Dolhem, F.; Deschamps, M.; Guyomard, D.; Poizot, P. A Rechargeable Lithium/Quinone Battery Using a Commercial Polymer Electrolyte. *Electrochem. Commun.* **2015**, *55*, 22–25. <https://doi.org/10.1016/j.elecom.2015.03.010>.
- (40) Lécuyer, M.; Deschamps, M.; Guyomard, D.; Gaubicher, J.; Poizot, P. Electrochemical Assessment of Indigo Carmine Dye in Lithium Metal Polymer Technology. *Molecules* **2021**, *26* (11), 3079. <https://doi.org/10.3390/molecules26113079>.
- (41) Mindemark, J.; Törmä, E.; Sun, B.; Brandell, D. Copolymers of Trimethylene Carbonate and ϵ -Caprolactone as Electrolytes for Lithium-Ion Batteries. *Polymer* **2015**, *63*, 91–98. <https://doi.org/10.1016/j.polymer.2015.02.052>.

- (42) Mindemark, J.; Sun, B.; Törmä, E.; Brandell, D. High-Performance Solid Polymer Electrolytes for Lithium Batteries Operational at Ambient Temperature. *J. Power Sources* **2015**, *298*, 166–170. <https://doi.org/10.1016/j.jpowsour.2015.08.035>.
- (43) Jouhara, A.; Dupré, N.; Gaillot, A.-C.; Guyomard, D.; Dolhem, F.; Poizot, P. Raising the Redox Potential in Carboxyphenolate-Based Positive Organic Materials via Cation Substitution. *Nat. Commun.* **2018**, *9* (1), 4401. <https://doi.org/10.1038/s41467-018-06708-x>.
- (44) Johansson, I. L.; Sångeland, C.; Uemiya, T.; Iwasaki, F.; Yoshizawa-Fujita, M.; Brandell, D.; Mindemark, J. Improving the Electrochemical Stability of a Polyester–Polycarbonate Solid Polymer Electrolyte by Zwitterionic Additives. *ACS Appl. Energy Mater.* **2022**, *5* (8), 10002–10012. <https://doi.org/10.1021/acsaem.2c01641>.
- (45) Zhang, B.; Liu, Y.; Pan, X.; Liu, J.; Doyle-Davis, K.; Sun, L.; Liu, J.; Jiao, X.; Jie, J.; Xie, H.; Sun, X. Dendrite-Free Lithium Metal Solid Battery with a Novel Polyester Based Triblock Copolymer Solid-State Electrolyte. *Nano Energy* **2020**, *72*, 104690. <https://doi.org/10.1016/j.nanoen.2020.104690>.
- (46) Lu, Y.; Zhang, Q.; Li, F.; Chen, J. Emerging Lithiated Organic Cathode Materials for Lithium-Ion Full Batteries. *Angew. Chem. Int. Ed.* **2023**, *62* (7), e202216047. <https://doi.org/10.1002/anie.202216047>.
- (47) Rambabu, D.; Lakraychi, A. E.; Wang, J.; Siew, L.; Gupta, D.; Apostol, P.; Chanteux, G.; Goossens, T.; Robeyns, K.; Vlad, A. An Electrically Conducting Li-Ion Metal–Organic Framework. *J. Am. Chem. Soc.* **2021**, *143* (30), 11641–11650. <https://doi.org/10.1021/jacs.1c04591>.
- (48) Wang, S.; Wang, L.; Zhang, K.; Zhu, Z.; Tao, Z.; Chen, J. Organic $\text{Li}_4\text{C}_8\text{H}_2\text{O}_6$ Nanosheets for Lithium-Ion Batteries. *Nano Lett.* **2013**, *13* (9), 4404–4409. <https://doi.org/10.1021/nl402239p>.
- (49) Jouhara, A.; Dupré, N.; Guyomard, D.; Lakraychi, A. E.; Dolhem, F.; Poizot, P. Playing with the P-Doping Mechanism to Lower the Carbon Loading in n-Type Insertion Organic Electrodes: First Feasibility Study with Binder-Free Composite Electrodes. *J. Electrochem. Soc.* **2020**, *167* (7), 070540. <https://doi.org/10.1149/1945-7111/ab7c6d>.
- (50) Bernard, L.; Jouhara, A.; Quarez, E.; Levieux-Souid, Y.; Le Caër, S.; Tran-Van, P.; Renault, S.; Poizot, P. Influence of Polymorphism on the Electrochemical Behavior of Dilithium (2,3-Dilithium-Oxy)-Terephthalate vs. Li. *Inorganics* **2022**, *10* (5), 62. <https://doi.org/10.3390/inorganics10050062>.
- (51) Hay, M. B.; Myneni, S. C. B. Structural Environments of Carboxyl Groups in Natural Organic Molecules from Terrestrial Systems. Part 1: Infrared Spectroscopy. *Geochim. Cosmochim. Acta* **2007**, *71* (14), 3518–3532. <https://doi.org/10.1016/j.gca.2007.03.038>.
- (52) Siew, L.; Lakraychi, A. E.; Rambabu, D.; Robeyns, K.; Jouhara, A.; Borodi, G.; Morari, C.; Poizot, P.; Vlad, A. Through-Space Charge Modulation Overriding Substituent Effect: Rise of the Redox Potential at 3.35 V in a Lithium-Phenolate Stereoelectronic Isomer. *Chem. Mater.* **2020**, *32* (23), 9996–10006. <https://doi.org/10.1021/acs.chemmater.0c02989>.
- (53) Nkosi, F. P.; Valvo, M.; Mindemark, J.; Dzulkurnain, N. A.; Hernández, G.; Mahun, A.; Abbrent, S.; Brus, J.; Kohera, L.; Edström, K. Garnet-Poly(ϵ -Caprolactone-*Co*-Trimethylene Carbonate) Polymer-in-Ceramic Composite Electrolyte for All-Solid-State Lithium-Ion Batteries. *ACS Appl. Energy Mater.* **2021**, *4* (3), 2531–2542. <https://doi.org/10.1021/acsaem.0c03098>.

- (54) Sun, B.; Mindemark, J.; Edström, K.; Brandell, D. Polycarbonate-Based Solid Polymer Electrolytes for Li-Ion Batteries. *Solid State Ion.* **2014**, *262*, 738–742. <https://doi.org/10.1016/j.ssi.2013.08.014>.
- (55) Sun, B.; Mindemark, J.; V. Morozov, E.; Costa, L. T.; Bergman, M.; Johansson, P.; Fang, Y.; Furó, I.; Brandell, D. Ion Transport in Polycarbonate Based Solid Polymer Electrolytes: Experimental and Computational Investigations. *Phys Chem Chem Phys* **2016**, *18* (14), 9504–9513. <https://doi.org/10.1039/C6CP00757K>.

Table of Contents graphic:

